



Understanding Permeability of Hydraulic Fracture Networks: A Preliminary Sandbox Analog Model

M.S. West Chester University of Pennsylvania

An Introduction to Understanding the Hydraulic Conductivity of Fracture Networks

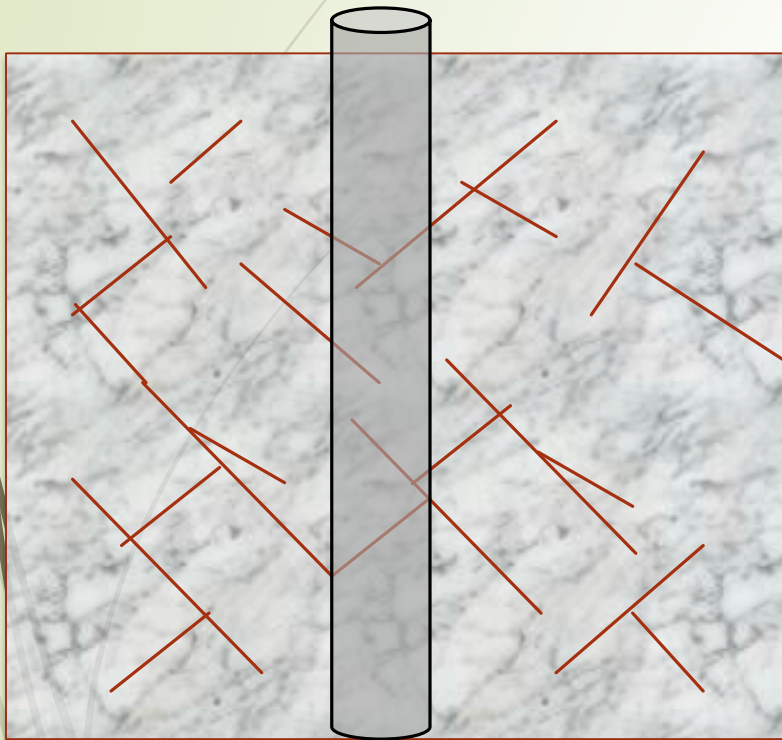


Figure 1: (A) Theoretical cross section with injection well to show how fracture network improves overall permeability of the matrix (Heldman, 2016).

- ▶ **Hydraulic fracturing** is the process by which a high-pressure fluid is injected into the low permeable rock layers to create fractures and fracture networks (Domenico & Schwartz, 1998).
- ▶ Generally, by **increasing the number of fractures** into the network, you increase its connectivity and **increase the permeability**
- ▶ Hydraulic fracturing fluid consists of several components:
 - ▶ Acids
 - ▶ Friction reducers
 - ▶ Gelling agents
- ▶ A **crosslinked gel** has a high viscosity (100-1000 cP or 0.1-1 Pas) and produce wider fractures and are frequently used in oil and high liquid wells (“Fracturing Fluids 101”, 2012)

Looking for answers in previous studies with models leaves us with more questions.

- ▶ Studies by Wang and Park (2002) showed how **permeability of rocks decreased with increasing effective confining pressure**
- ▶ Gangi (1978) too showed that generally, **permeability decreases with increasing normalized confining pressure**
- ▶ Walsh (1981) found **permeability of the fracture increases with increasing effective pressure**
- ▶ Li et al., (1994, 1997) found that **confining pressure and pore pressure have the greatest influence on permeability in the “strain-softening” region and only play a role in units with very high permeability**

To grasp the complexity of changes to permeability from a fracture network, a “sandbox” model based on Galland et al. (2006) research will be utilized.

- Scaling relationships for brittle rocks that fail according to the Mohr-Coulomb criterion only two parameters need to be described: **cohesion** (C) and **the coefficient of internal friction** (μ) (Hubbert, 1937)
- Sand, and other **fine grained** dry materials, have **small cohesion** values and **similar coefficients of internal friction to that of brittle crust** and make good modeling materials (Hubbert, 1937)
- Sand however tends to fluidize and not fracture and was not used in this study



High Viscosity Hydraulic Fracturing Fluid Analogue – Crisco © Vegetable Shortening



(Stokes Law, 1851)

$$\mu = 2 (\rho_{\text{sphere}} - \rho_{\text{liq}}) g r^2 / (9 V)$$

ρ_{sphere} – density of clay sphere (g/mL)

ρ_{liq} – density of liquid at 50°C (g/mL)

g – gravity (cm/s²)

r –radius (cm)

V - velocity (cm/s)

	Temperature (°C)	Density (g/mL)	Viscosity (g/cm • s)	Viscosity (Pa • s)
Solid Vegetable Shortening	31	0.9018	-	-
Liquid Vegetable Shortening Mixture	50	0.9009	1.126	0.1126
Liquid Vegetable Shortening Mixture	40	0.8595	4.381	0.4381

Table 1: Properties of the Crisco © All-Vegetable shortening, density and viscosity were calculated based on methods mentioned (Heldman, 2016).

Low Permeability Shale Analogue – Highly Angular Silica Flour #325

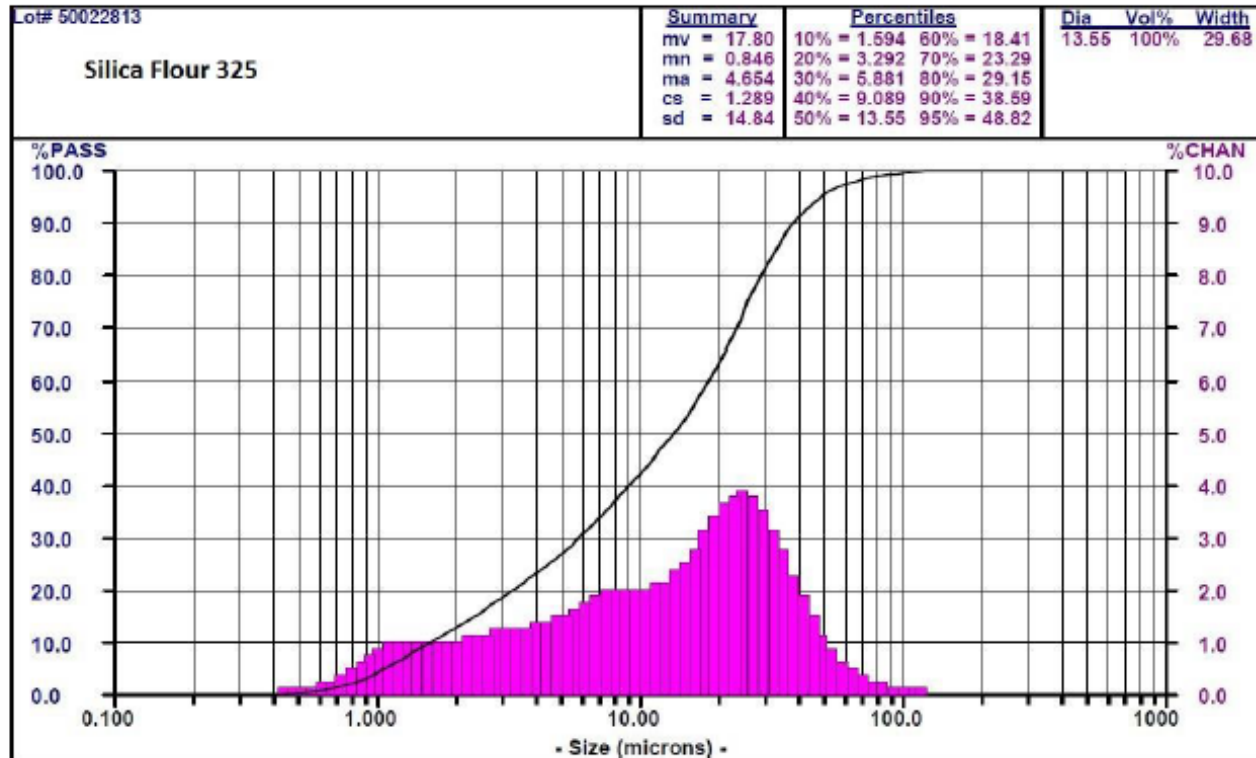


Figure 3: Grain size distribution for AGSCO #325 Silica Flour. Mean Volume ~17.80 microns (AGSCO #325 Silica Flour Technical Sheet, 2013).

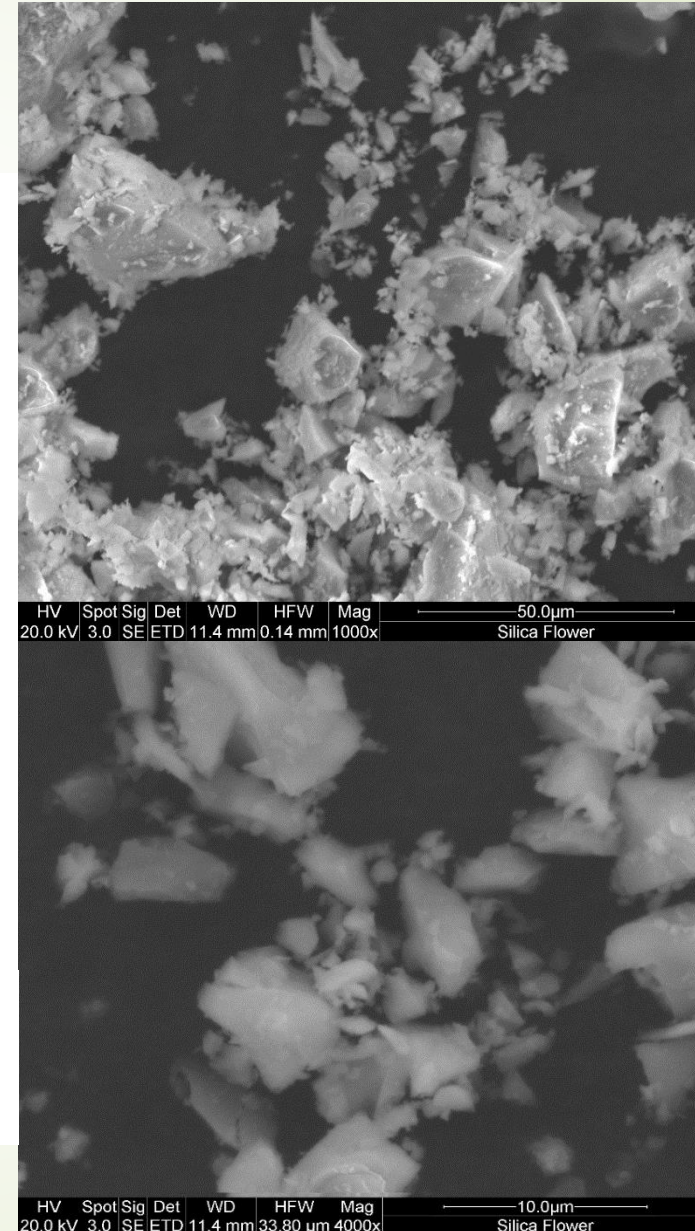


Figure 4 A and B (top and bottom): Micrographs of Silica Flour #325 taken with a scanning electron microscope (SEM), **A** at 50 microns and **B** at 10 microns. High power magnification shows the highly angular shape of the silica flour, similar to that of the SI-CRYSTAL of the Galland et al. (2006) research (Heldman, 2016).

Initial hydraulic conductivity testing yields values similar to that of silt ($10^{-6} - 10^{-4}$ cm/s).

(Fetter, 2001)

$$k = \frac{d_r^2 \cdot L}{d_c^2 \cdot t} \cdot \ln \frac{H_o}{H_t} = 0.003 \text{ cm/s}$$

- d_r – diameter of the vertical column (cm)
- L – length of the sample in the housing chamber (cm)
- d_c – diameter of the sample in the housing chamber (cm)
- t – time between H_o and H_t (s)
- H_o – initial “head” (cm)
- H_t – final “head” (cm)

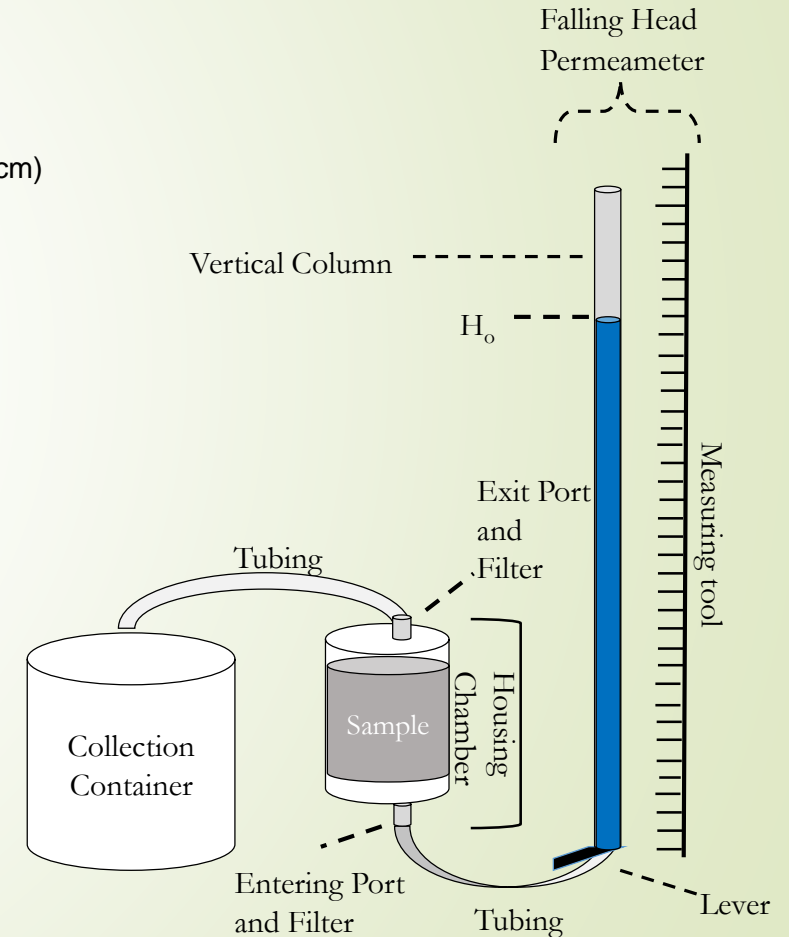
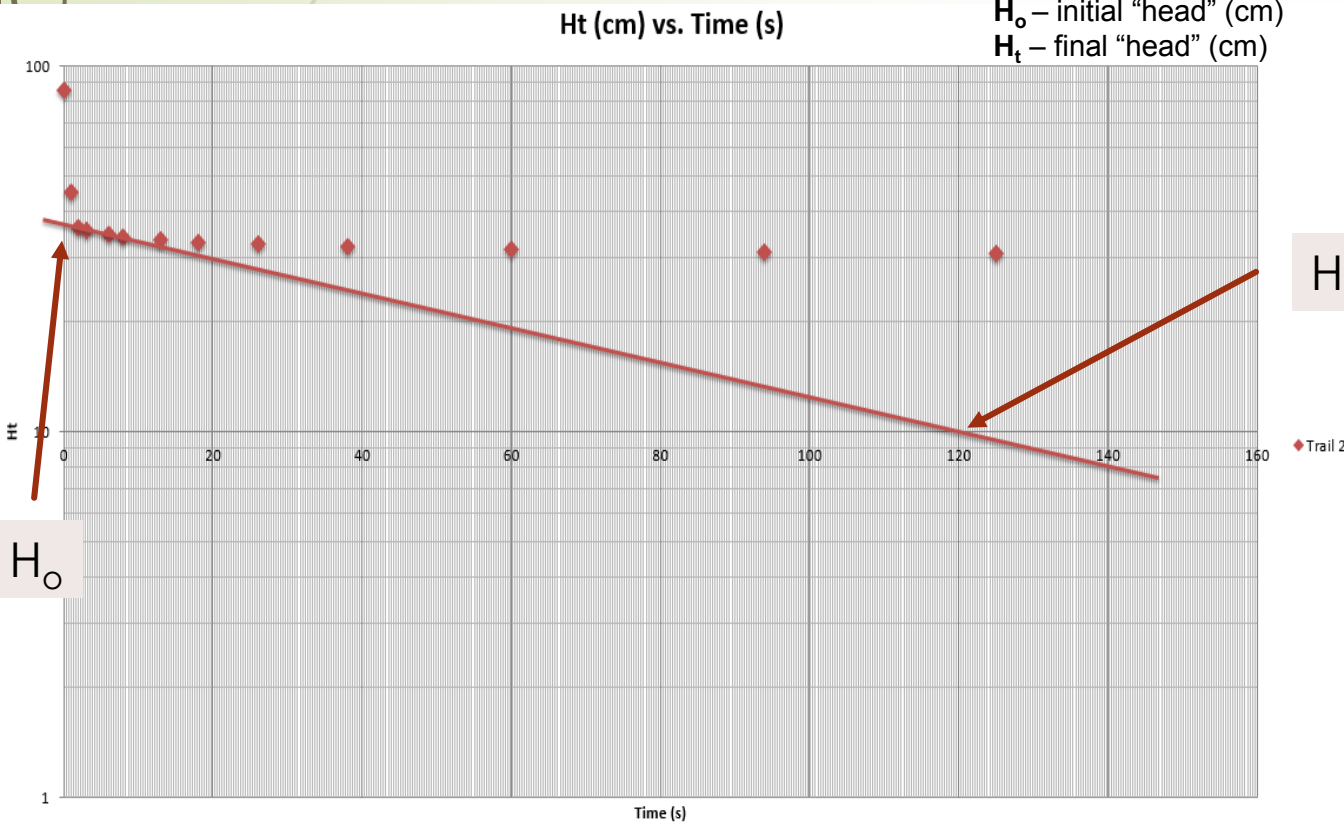


Figure 5: Schematic of Falling Head Permeameter Testing Apparatus (Heldman, 2016).

Preliminary testing apparatus for shear testing yields cohesion value of ~105 Pa.

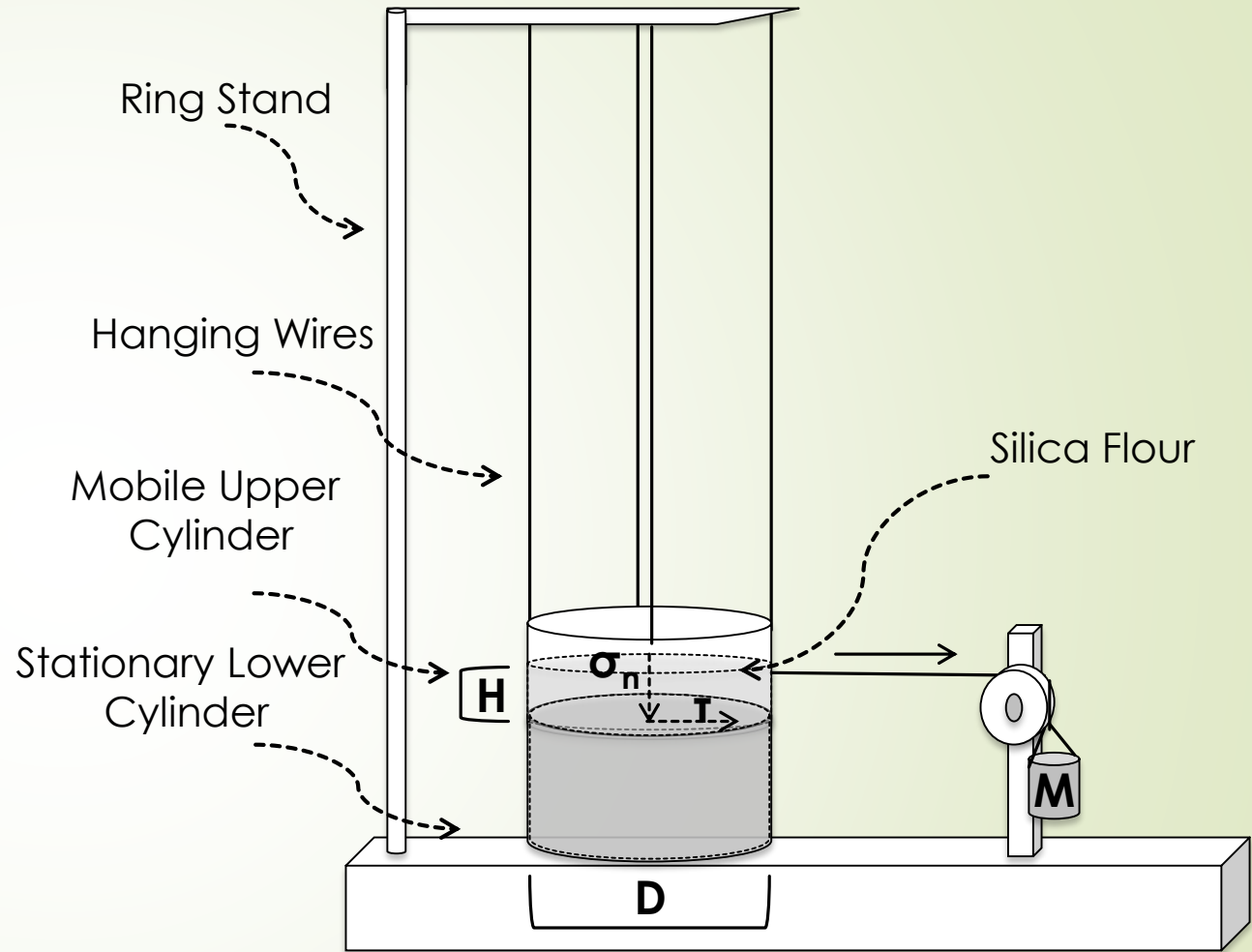


Figure 6 A and B (left to right): (A) Photo of apparatus. **(B)** Schematic of shear testing apparatus. Silica flour was slowly poured into upper and lower cylinders using a 1 tablespoon scoopula and then packed systematically for compacted silica trials. Failure was calculated when mass (M) caused a $\geq 3\text{mm}$ slip in the upper cylinder. Solid arrows indicate direction of motion (Heldman, 2016).

Preliminary testing apparatus for tensile strength yields value of ~40 Pa.



Top View Of Tensile Schematics

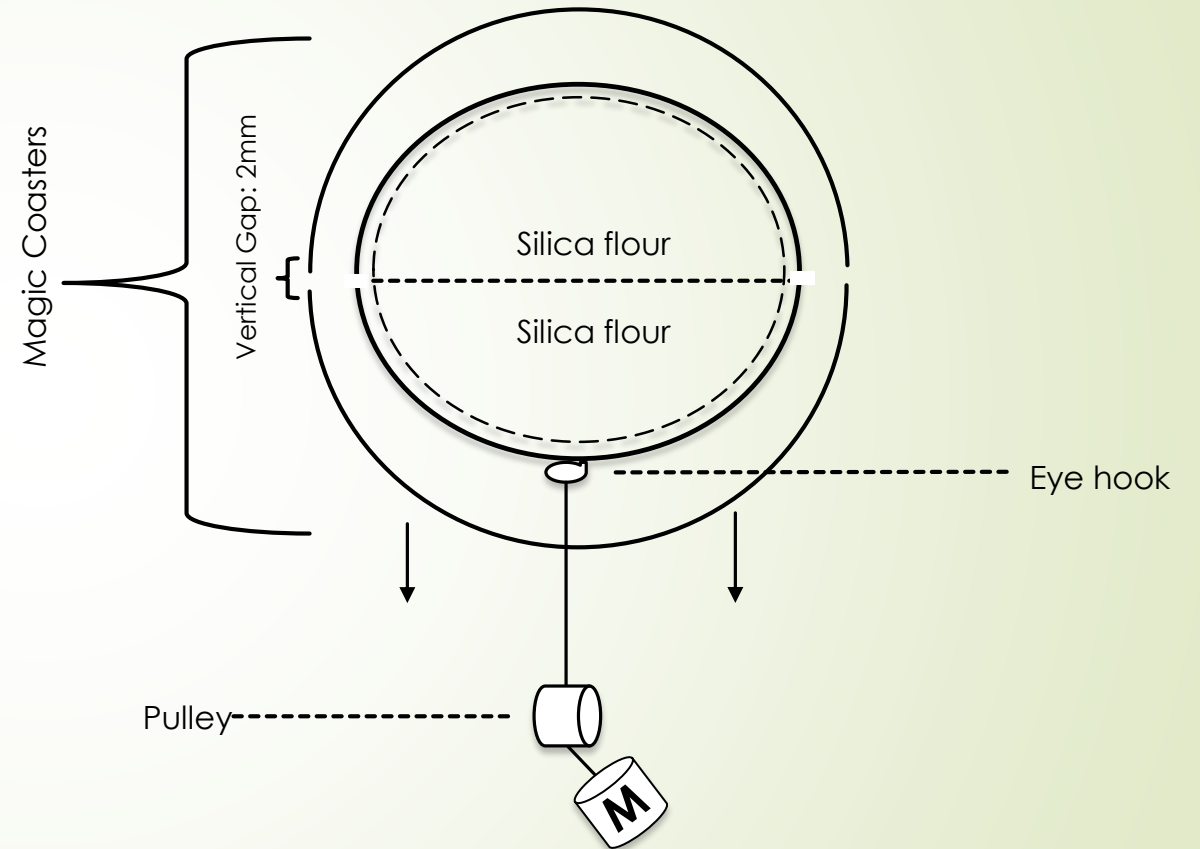
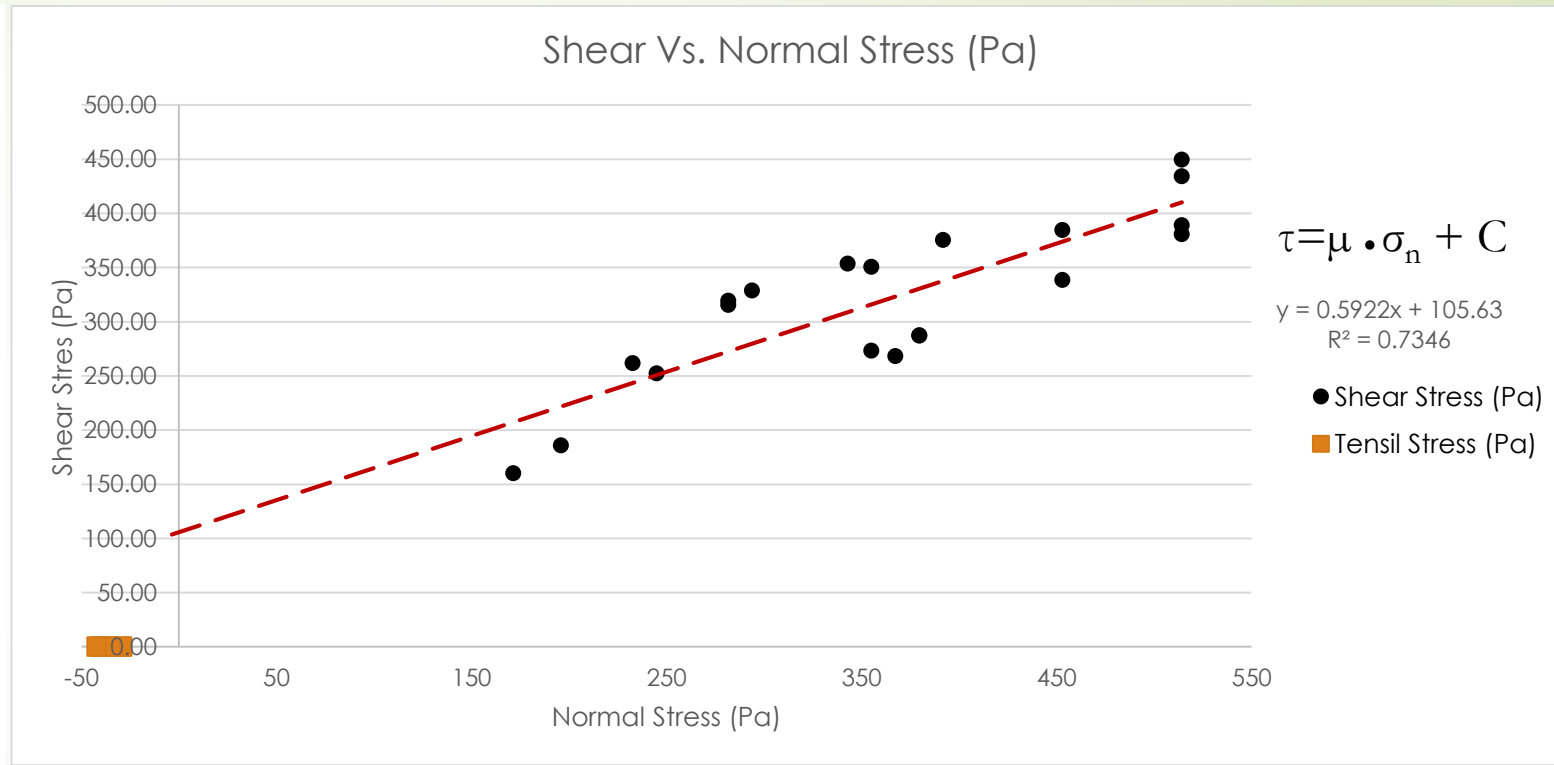
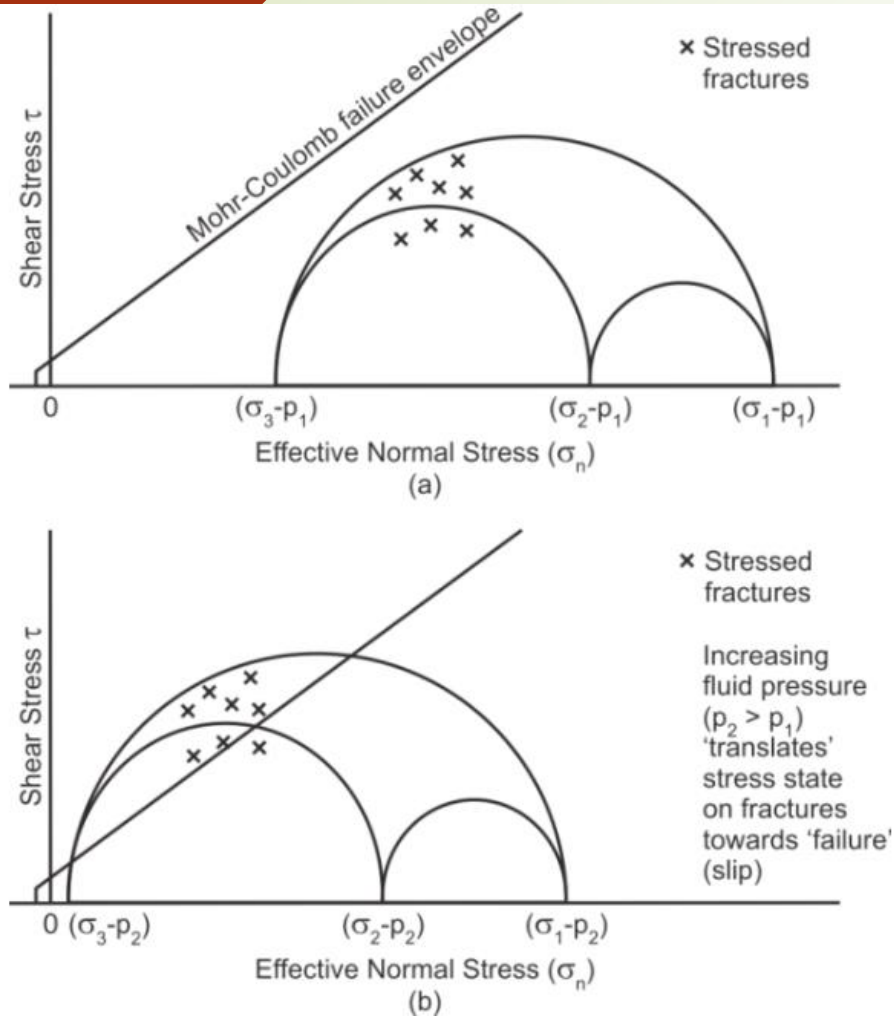


Figure 7 A and B: (A) Photo of apparatus. (B) Schematic of tensile strength testing apparatus. Silica flour was slowly poured into the two half cylinders using a 1 tablespoon scoopula and then packed systematically for compacted silica trials. Failure was calculated when mass (M) caused a $\geq 3\text{mm}$ slip in the mobile cylinder. Solid arrows indicate direction of motion.

Graphing Shear and Tensile Strength vs. Normal Stress yields a Mohr-Coulomb failure envelope which gives us the value of friction (μ) and cohesion (C).



Source	Particle d (μm)	ρ (g/cm^3)	C (Pa)	T (Pa)	μ
Galland et al. (2006)	SI-CRYSTAL ~10-20	$1.33 \pm 0.2\%$	288 ± 26	88 ± 17	$0.840 \pm$
	SI-SPHERE ~30	$1.56 \pm 0.18\%$	1.5	Negligible	0.042
Experiment	#325 Si Flour ~17.8	1.25	105.63	40.32	0.5992

Figure 8 A and B (left to right): (A) Mohr-Coulomb failure envelope showing how hydraulic fracturing shifts the Mohr circle to the left (Charles Fairhurst, 2013). (b) Graph of Shear vs. Normal stress where the linear line represents the Mohr-Coulomb failure envelope of failure of AGSCO #325 silica flour (Heldman, 2016).

The following “sandbox” model was used for 14 injection trials at different confining pressures and with high and low viscosity injection fluid.

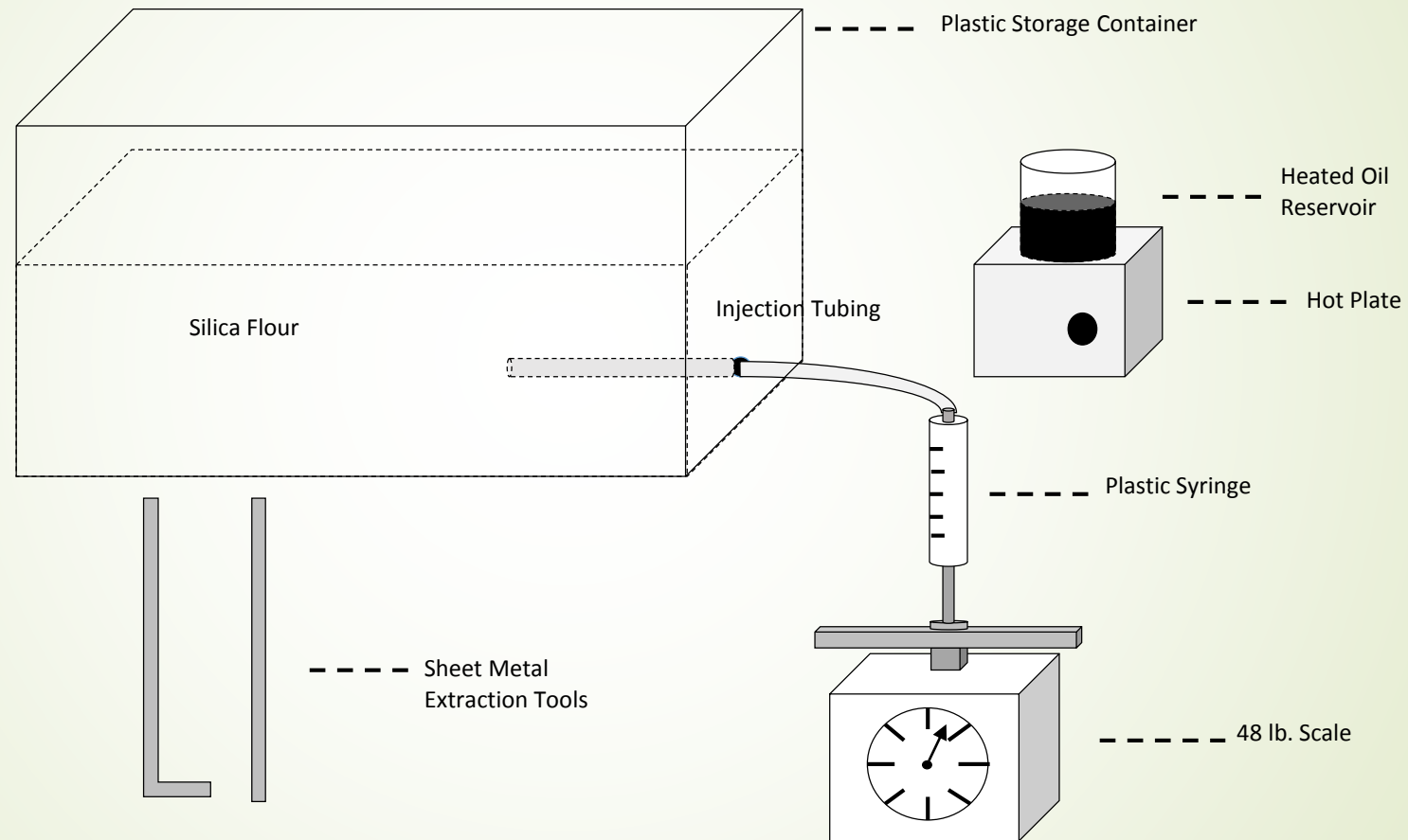
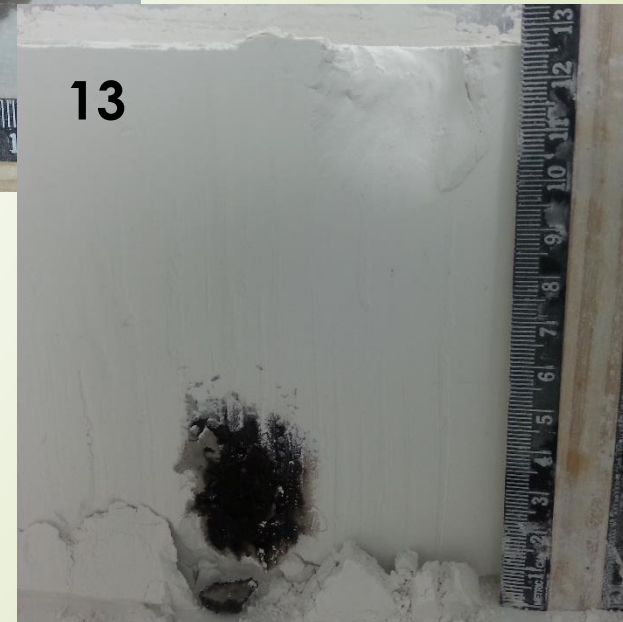


Figure 9: Principal Testing Apparatus. Oil is extracted from the reservoir using injection tubing connected to the plastic syringe and injected into the silica flour housed in the plastic storage container. Pressure of injection are read from the scale as the tester pushed down on the plunger during injection. Once solidified, the samples are then extracted using the sheet metal extraction tools in ~1” cross sections (Heldman, 2016).

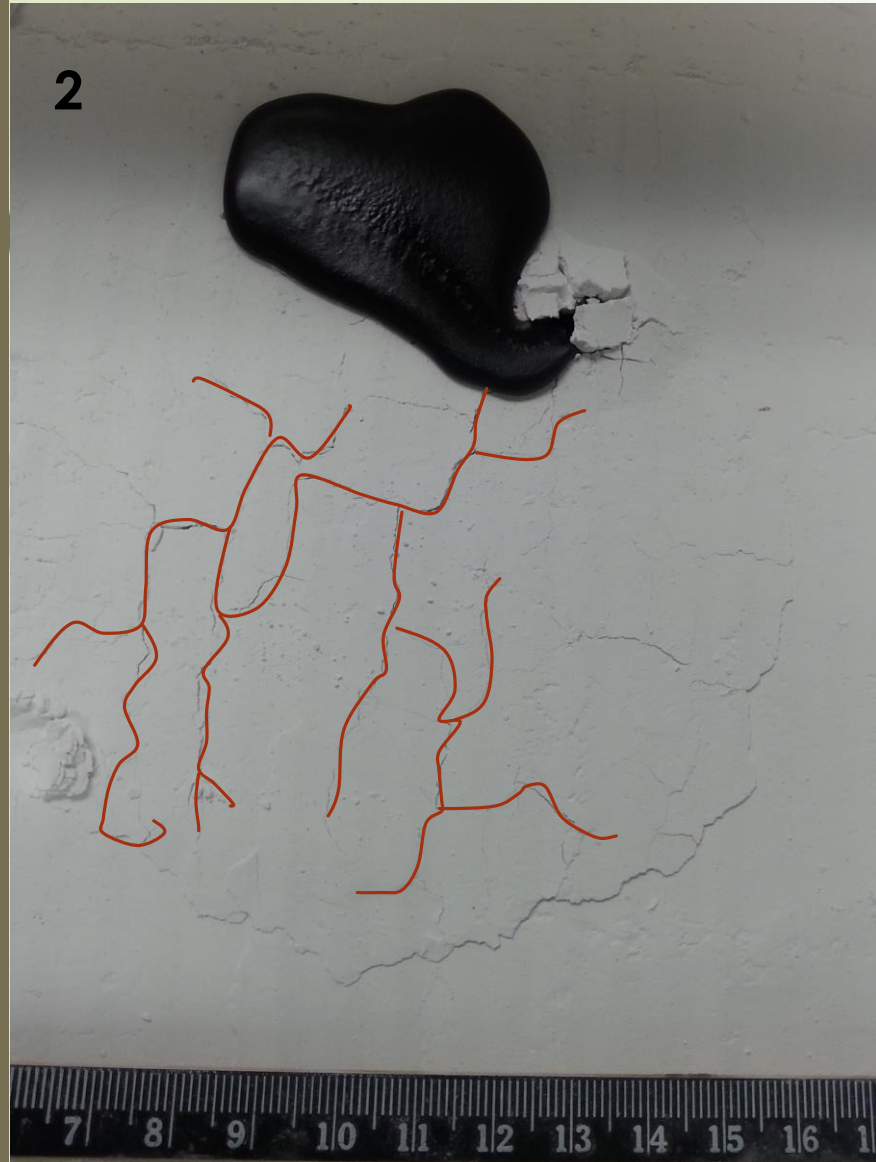
Procedural Steps for Primary Testing



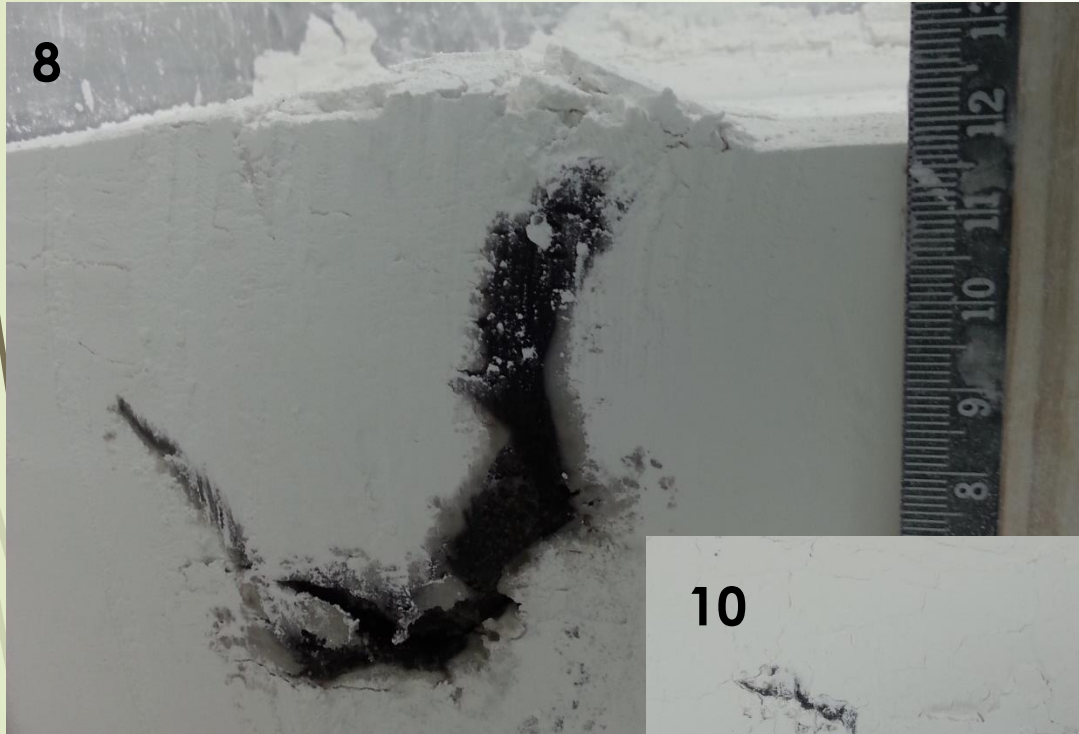
Notable Trials - Trail 1, 4 and 13 all displayed back filling and pooling of the injection fluid near the injection port without fractures.



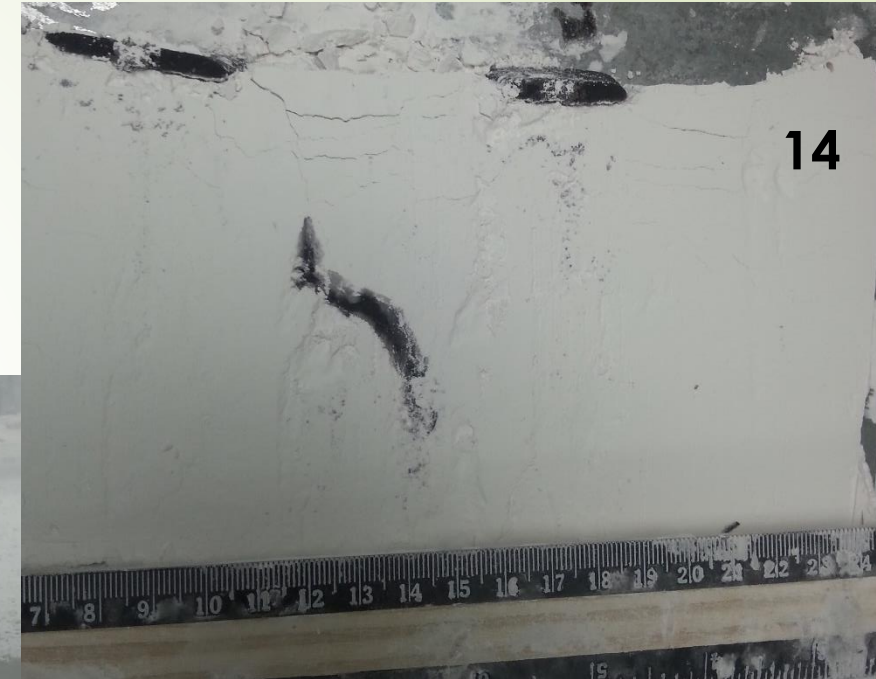
Notable Trials – Many of the trials exhibited surface rupture and some developed divergent faulting!



Notable Trials- Good fracture development occurred when the viscosity of the injection fluid was increased.



Notable Trials- Some trials developed some interesting fracture networks full of dikes and sills.



Using some mathematical analysis we can quantify the change in the permeability of the matrix. The largest primary fracture for each trial was used in analysis excluding trails 1, 4, and 13.



Figure 10: Measurements taken for calculating the hydraulic conductivity of the fracture using the *cube law*, b is fracture aperture (Heldman, 2016).

By using the *cube law* equation we can estimate the hydraulic conductivity of the fracture (Snow, 1965):

$$k_f = \frac{b^3 \rho g N}{12 \nu B} \quad \text{yielded values from } 0.06 - 36.9 \text{ cm/s}$$

- b – fracture aperture (cm)
- ρ – density in (g/cm^3)
- ν – viscosity of fracturing fluid (g/cms)
- g – gravity (cm/s^2)
- N – number of fractures (assumed 1)
- B – fracture spacing (assumed 1)

And convert this into permeability (Fetter, 2001):

$$K = k \cdot (\nu / (\rho \cdot g)) \quad \text{yielded average value of } 0.0315 \text{ cm}^2$$

- K – permeability if unit (cm^2)
- k – hydraulic conductivity (cm/s)
- ρ – density (g/cm^3)
- ν – viscosity (g/cms)
- g – gravity (cm/s^2)

During testing, it was noticed that the fracture pressure was highly dependent on the confining pressure and the viscosity of the injection fluid.

Critical Pressure and Injection Pressure vs. Normal Pressure

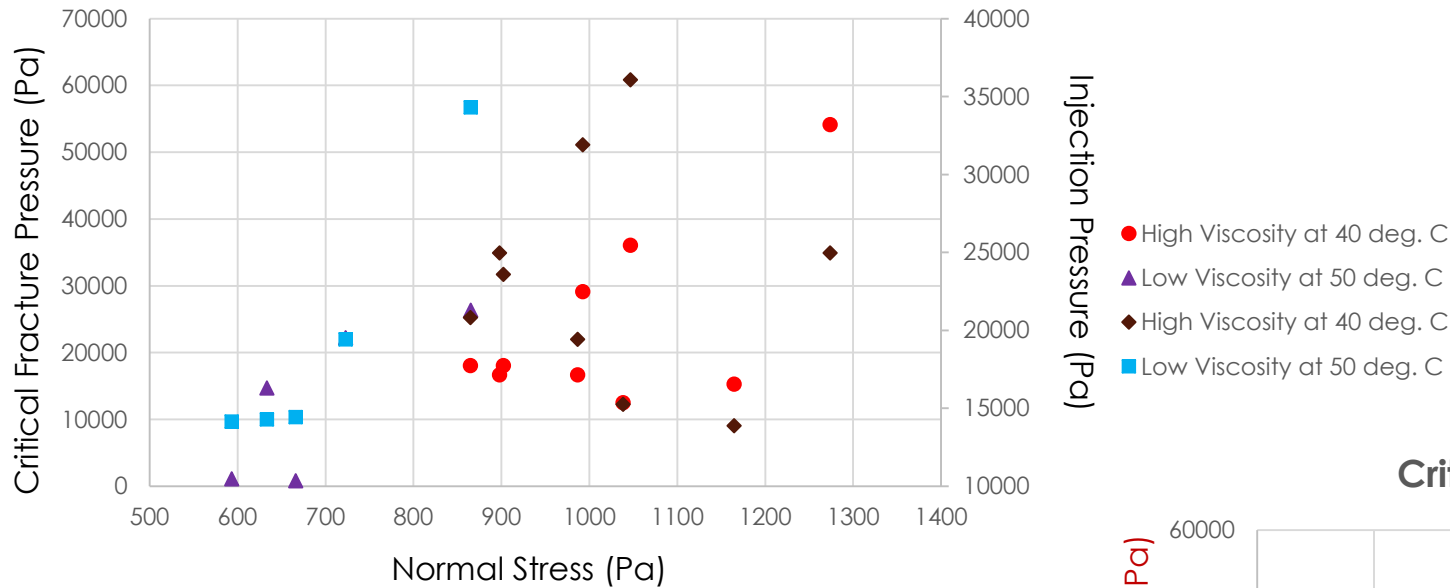
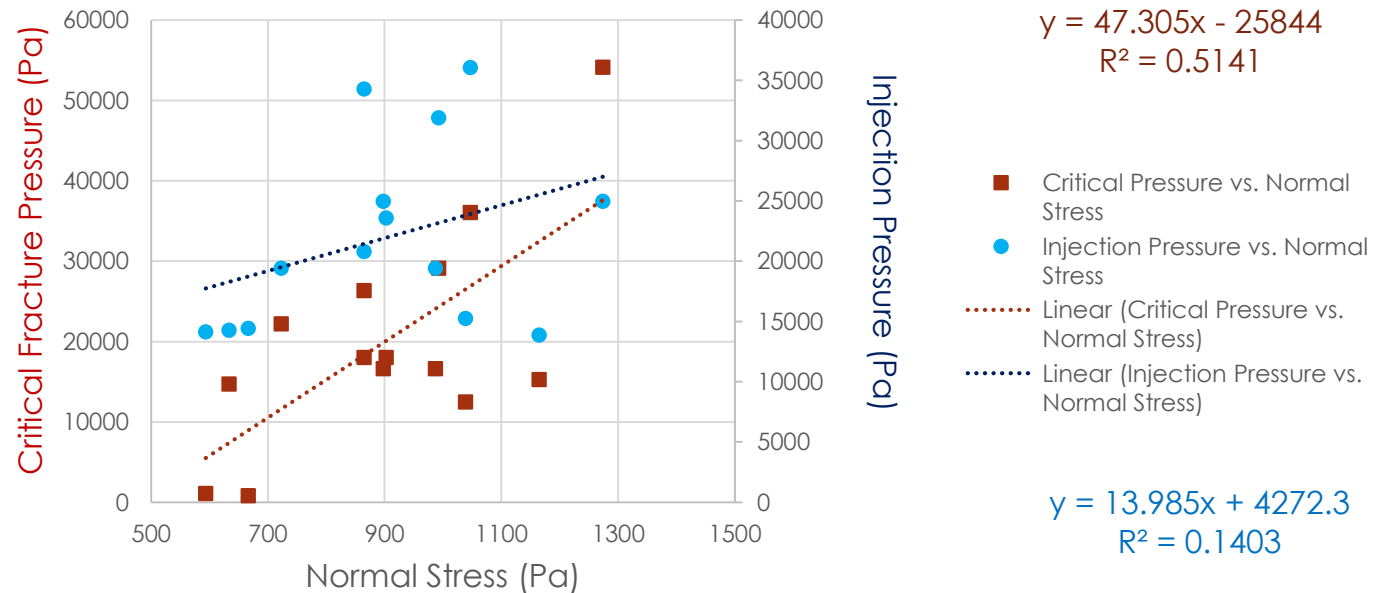


Figure 11 A and B (left to right): (A) Graph of Critical & Injection Pressure vs. Normal Stress at different viscosities, (B) Graph of Critical & Injection Pressure vs. Normal Stress showing a positive relationship between these parameters (Heldman, 2016).

Critical and Injection Pressure vs. Normal Stress



Additionally, a positive relationship between fracture length, fracture permeability and normal stress was achieved for the high viscosity trials

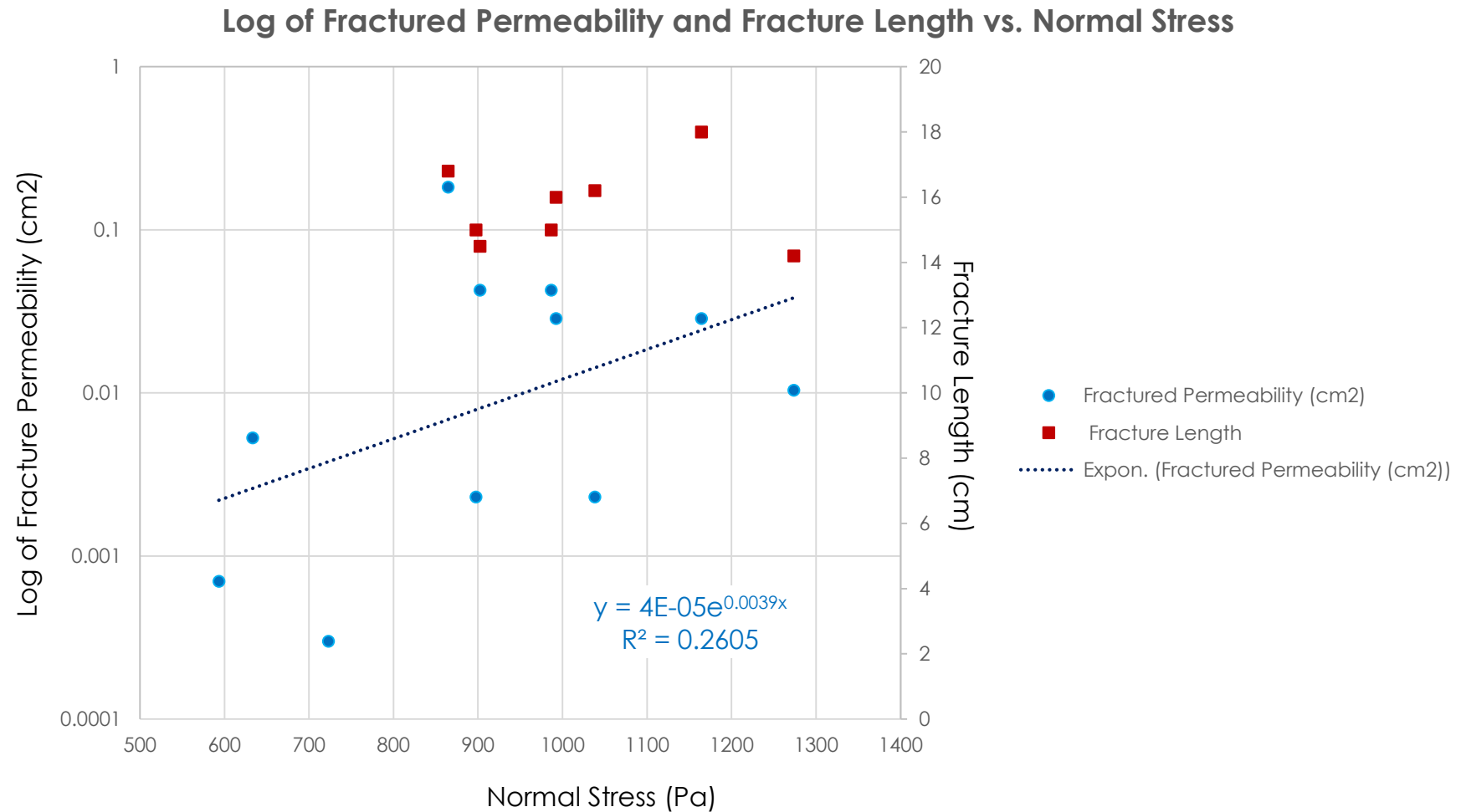
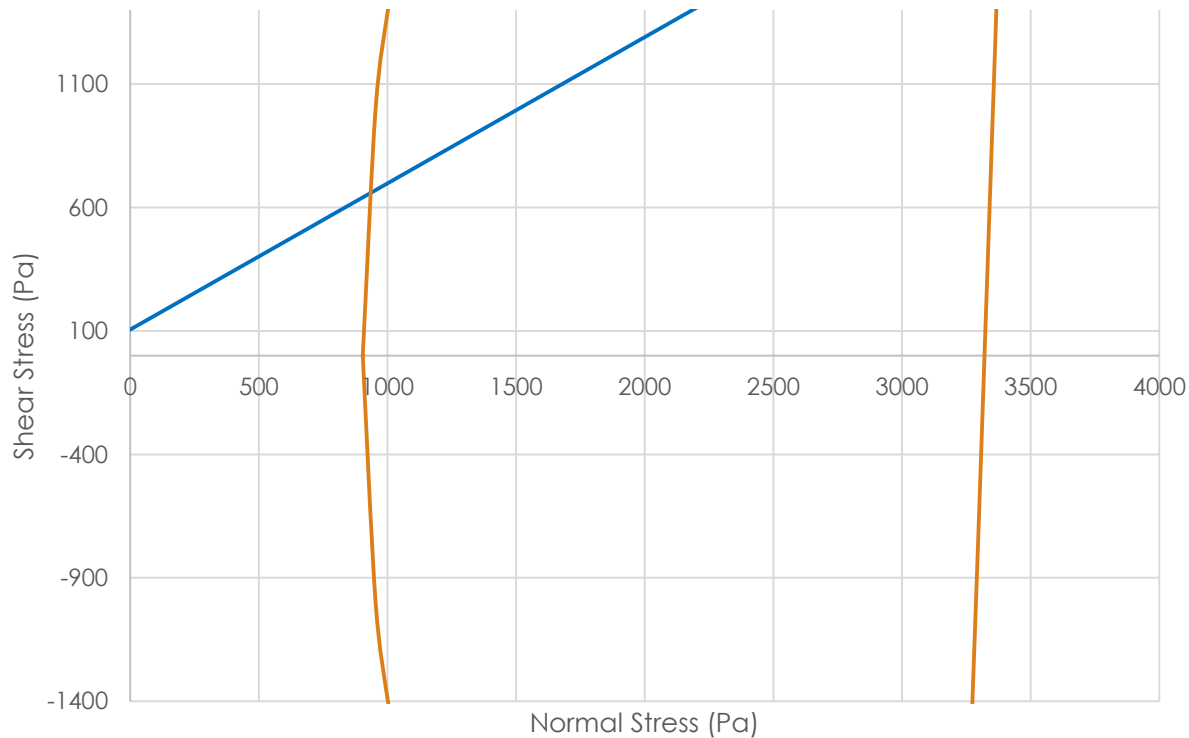


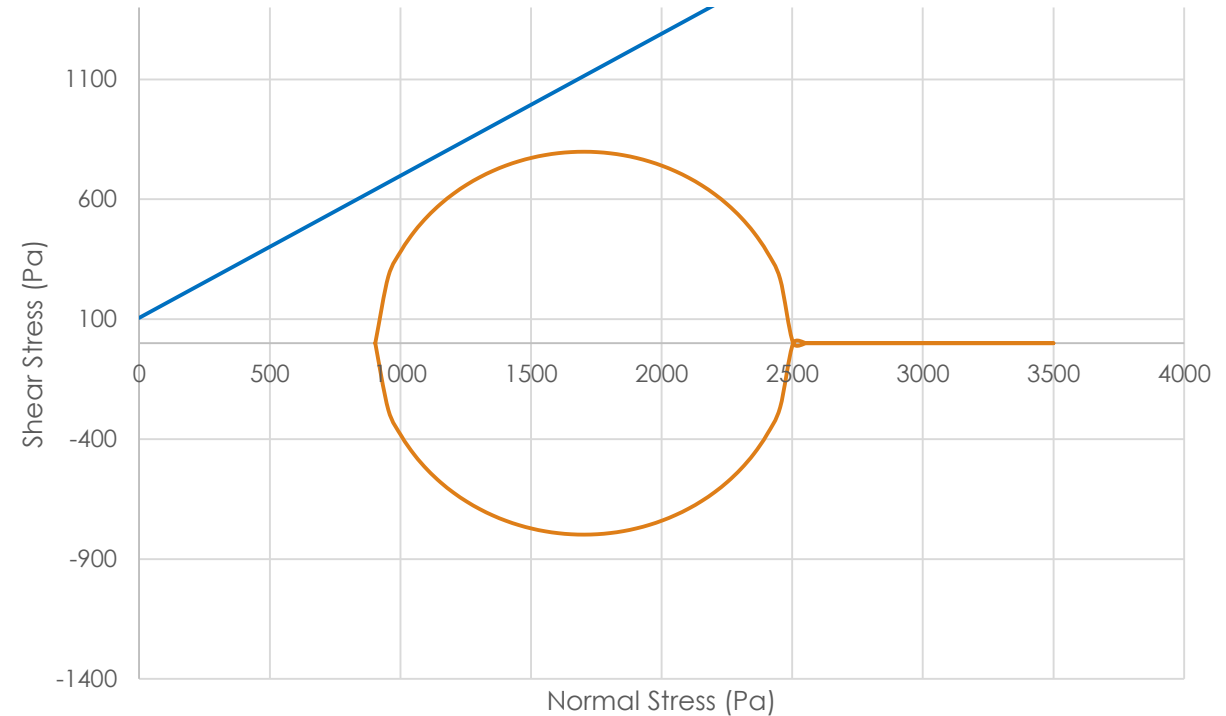
Figure 12: Graph of the Fracture Permeability and Fracture length vs. Normal stress on a semi-log axis after outlying points are removed. A positive relationship was seen between the fracture permeability (log axis) and slight positive relationship between the length of fracture and normal stress (Heldman, 2016).

Drawing a Mohr-Coulomb diagram for the critical injection pressure illustrates some issues with our values.

Mohr-Coulomb Failure Envelope for Critical Fracture Pressure (kg/m²)



Mohr-Coulomb Failure Envelope for Critical Fracture Pressure (kg/m²)



When the fluid pressure exceeds the tensile strength of the rock, rupture will occur. Observations by Handlin (1963) found that the pressure (P_{critical}) needed for critical failure of sedimentary rocks is 80% of the normal stress (σ): $P_{\text{critical}} = 0.8 \sigma$. Values from the critical fracture pressure are much higher!

Several sources of error may come into play to explain the vast differences between trials.

- (1) the confining pressure and density of the silica flour varied for each trial
- (2) the temperature of the injection fluid was a rough estimate
- (3) some silica flour was reused between trials
- (4) injection rate was not accounted for
- (5) trials were conducted over several days and some silica samples were left open in the ambient laboratory
- (6) critical pressure could be high if silica flour clogged the injection tubing

Why are we interested in determining the change in permeability and what is Oklahoma's new "seismic" predicament?

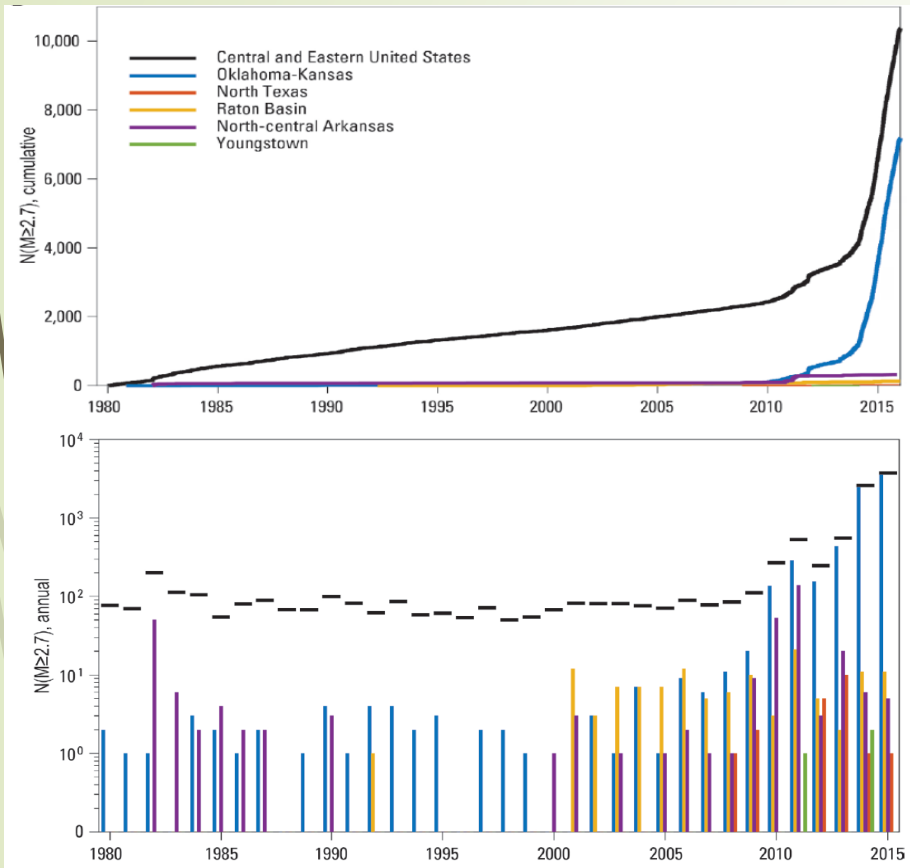


Figure 2 A and B (top and bottom): (A) Map showing locations of oil and gas plays and sedimentary basins associated with induced seismicity (U.S. Energy Information Administration, 2015; Weingarten and others, 2015). (B) Cumulative (top) and annual counts (bottom) of M2.7 and greater earthquakes in the Central and Eastern United States (CEUS) and five select zones of induced seismicity since 1980 (Petersen and others, 2014).

- Seismicity introduces compression and extensional processes of **stress** and **strain** which can further fracture development and **potentially increase matrix permeability**.
- Levels of seismicity have **increased in Oklahoma** from **wastewater injection** from oil and gas production.
- Increased seismicity could introduce **more fractures** or **further fracture development** in the matrix and potentially **increase the spread of contaminants**.



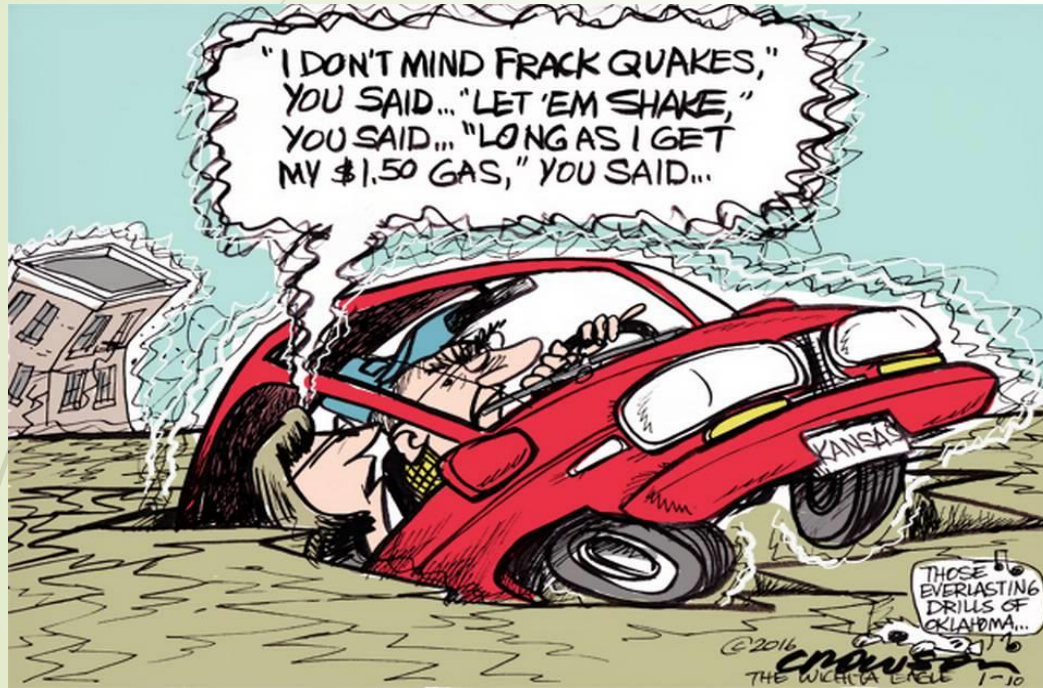
Figure 3: Picture of damage related to Nov. 2011 seismic event (<https://watchers.news/2011/11/06/5-6-magnitude-oklahoma/>)

Conclusions and Further Investigations

- **development of the fracture network was highly dependent on the confining pressure and viscosity of the injection fluid**
- **general positive relationship was illustrated between the confining pressure, the viscosity and the horizontal fracture length due to increased propagation**
- **The hydraulic conductivity of the fracture average was 6.7 cm/s from 2.7×10^{-4} cm/s of initial hydraulic conductivity of silica flour**
- **average permeability of the fracture was 0.032 cm^2 ; increased from $2.7 \times 10^{-9} \text{ cm}^2$ of the pre-fractured matrix, increase of**
- **positive relationship was found between the confining pressure and permeability of the fractured matrix**

- Concern in Oklahoma with its increase is seismicity as a potential force to increase permeability and extend contamination
- With the average permeability calculations, one could attempt to track potential contamination of the fracturing fluid if released into the central Oklahoma formation
- Calculate how long it would take the substance to reach nearby groundwater aquifers and quantify any potential of increased contamination from the highly fractured formations

I would like to acknowledge the following people:



http://www.kansas.com/latest-news/oqmetj/picture53992420/ALTERNATES/FREE_960/crowson%201-10-16.jpg

- I would like to thank Dale Lynch for his assistance in preliminary and primary testing procedures.
- Peter Hornbach for his assistance in the collection of SEM images.
- I would also like to thank Dr. Martin Helmke for his assistance in hydraulic conductivity and permeability calculations.
- My advisor Dr. Howell Bosbyshell for his assistance in the creation of testing materials, testing procedures and continued guidance throughout the preparation of this study.

References

AGSCO #325 Silica Flour Technical Sheet, 2013.

Charles Fairhurst (2013). Fractures and Fracturing - Hydraulic fracturing in Jointed Rock, Effective and Sustainable Hydraulic Fracturing, Dr. Rob Jeffrey (Ed.), InTech, DOI: 10.5772/56366

Domenico, P., & Schwartz, F. (1998). Hydraulic Conductivity and Permeability of Geologic Materials. In *Physical and chemical hydrogeology* (2nd ed.). New York: Wiley.

Fetter, C. (2001). Properties of Aquifers. In *Applied Hydrogeology* (4th ed.). Upper Saddle River, New Jersey: Prentice Hall.

"Fracturing Fluids 101". (2012). Retrieved June 7, 2016, from <http://www.hexionfracline.com/fracturing-fluids-101>

Galland, O., Cobbold, P. R., Hallot, E., de Bremond d'Ars, J., & Delavaud, G. (2006). Use of vegetable oil and silica powder for scale modelling of magmatic intrusion in a deforming brittle crust. *Earth and Planetary Science Letters*, 243(3), 786-804.

Handin, J. (1969). On the Coulomb–Mohr failure criterion. *Journal of Geophysical Research*, 74 (1969), pp. 5343–5348

Hubbert, M. K. (1937). Theory of scale models as applied to the study of geologic structures. *Geological Society of America Bulletin*, 48(10), 1459-1520.

Petersen, M. D., Mueller, C. S., Moschetti, M. P., Hoover, S. M., Llenos, A. L., Ellsworth, W. L., ... & Rukstales, K. S. (2016). 2016 One-Year Seismic Hazard Forecast for the Central and Eastern United States from Induced and Natural Earthquakes (No. 2016-1035). US Geological Survey.

Snow, D.T. (1965) A parallel plate model of fractured permeable media. PhD Thesis Univ. of Calif., Berkeley.

Image:

<https://watchers.news/2011/11/06/5-6-magnitude-oklahoma>

http://www.kansas.com/latest-news/oqmetj/picture53992420/ALTERNATES/FREE_960/crowson%201-10-16.jpg

Trail Number	Weight of Silica Flour (lbs)	Weight of silica Flour (kg)	Height of silica Flour (cm)	Height of Silica Flour (m)	Height For Normal Stress (m)	Density (kg/m ³)	Density (g/cm ³)	Normal Stress (Pa)	Critical Fracture Pressure (kg/cm ²)	Critical Pressure (kg/m ²)	Ratio of Critical to Normal	Critical Fracture Pressure (Pa)	Injection Pressure (kg/cm ²)	Injection Pressure (Pa)	Greatest Length of Fracture (cm)
1	26.5	12.0	11.4	0.11	0.079	1115.98	1.12	864.88	0.27	2687.95	3.11	26368.80	0.35	34296.56	22.4
2	20.8	9.4	9.9	0.10	0.064	1008.66	1.01	633.28	0.15	1499.59	2.37	14711.01	0.15	14289.78	18.3
3	20.2	9.2	9.3	0.09	0.058	1042.76	1.04	593.31	0.11	1131.77	1.91	11102.65	0.14	14151.05	17
4	22.0	10.0	9.8	0.10	0.063	1077.74	1.08	666.07	0.08	848.83	1.27	8326.99	0.15	14428.52	17.3
5	23.3	10.5	10.3	0.10	0.068	1083.68	1.08	722.90	0.23	2263.54	3.13	22205.30	0.20	19423.00	14.7
6	27.0	12.2	11.9	0.12	0.084	1089.26	1.09	897.60	0.17	1697.65	1.89	16653.98	0.25	24972.43	15
7	35.5	16.1	14.7	0.15	0.112	1159.38	1.16	1273.84	0.55	5517.37	4.33	54125.42	0.25	24972.43	14.2
8	25.5	11.6	12.5	0.13	0.090	979.37	0.98	864.69	0.18	1839.12	2.13	18041.81	0.21	20810.36	16.8
9	32.3	14.6	15.0	0.15	0.115	1032.18	1.03	1164.45	0.16	1556.18	1.34	15266.15	0.14	13873.57	18
10	30.0	13.6	13.2	0.13	0.097	1091.10	1.09	1038.26	0.13	1273.24	1.23	12490.48	0.16	15260.93	16.2
11	28.0	12.7	13.9	0.14	0.104	967.07	0.97	986.65	0.17	1697.65	1.72	16653.98	0.20	19423.00	15
12	26.0	11.8	13.3	0.13	0.098	938.51	0.94	902.26	0.18	1839.12	2.04	18041.81	0.24	23585.08	14.5
13	30.0	13.6	13.5	0.14	0.100	1066.85	1.07	1046.58	0.37	3678.25	3.51	36083.62	0.37	36071.29	12.6
14	29.0	13.2	12.8	0.13	0.093	1087.69	1.09	992.33	0.30	2970.89	2.99	29144.46	0.33	31909.22	16
Average	26.9	12.2	12.3	0.12	0.088	1052.87	1.05	903.76	0.22	2178.65	2.41	21372.60	0.22	21961.95	16.28571429